Interactions of Coupled Acoustic and Vortical Instability

T. J. Chung* and J. L. Sohn†
University of Alabama, Huntsville, Alabama

Unstable waves may occur as a result of acoustic and/or vortical (hydrodynamic) oscillations. If these two different types of waves are coupled together, their physical interactions lead to extremely complicated phenomena. Theoretically, there exists an infinite number of frequencies for both acoustic and hydrodynamic oscillations. Realistically, however, only a limited number of combined frequencies are excited. Our objective is, then, to determine the combined nature of acoustic and hydrodynamic frequencies at which instabilities may arise. This subject is important in rocket motor chambers when the vortical field is coupled with acoustic pressure oscillations. In the past, the acoustic combustion instability was studied independently of the hydrodynamic instability induced by vortex motions. This paper is intended to combine the two different sources of energy everywhere within the spatial domain and determine the effect of one upon the other. This can be achieved by calculating the mean flow velocities and vorticities and their fluctuating parts of velocities and vortices, as well as the fluctuating pressure. To elucidate this coupling mechanism, however, a very simple model is first introduced. The Orr-Sommerfeld equation is utilized to determine the wavenumbers and unsteady stream functions from which vortically coupled acoustic instability growth constants are calculated. This process demonstrates that there are two different frequencies, acoustic and hydrodynamic, various combinations of which contribute to either damping or amplification. Finally, the limitation of the Orr-Sommerfeld equation is removed by numerical solution of the perturbed vorticity transport equation using finite elements. It is found that stability boundaries for coupled acoustic and vortical oscillations are somewhat similar to the classical hydrodynamic stability boundaries, but they occur in the form of multiple islands.

Nomenclature

A = admittance at the burning surface, $=A^{(R)}+iA^{(I)}$
a = sonic velocity ($\gamma P_0/\rho_0$)
c = phase velocity (real part), growth constant (imaginary part), $=c^{(R)}+ic^{(I)}$
c_p = specific heat at constant pressure
L = length of the combustion chamber
k = complex wavenumber ($\omega-i\alpha$)
k^* = complex vortical wavenumber
k = vortical wavenumber
M = Mach number
P = pressure
Re = Reynolds number ($\rho_0 aL/\mu$)
S = Strouhal number
T = temperature
t = time
u_i = velocities
x_i = spatial coordinates
α = growth constant
ϵ = perturbation parameter
ϵ_{ijk} = permutation symbol
ϕ = amplitude of stream function
Φ = finite element trial (interpolation) function
ξ_i = vorticities
ρ = density
ψ = stream function
γ = specific heat ratio
μ = viscosity
Γ = boundary
Ω = domain

Subscripts and Superscripts

$(\,)'$ = acoustic fluctuation
$(\,)^*$ = vortical fluctuation
A = acoustic component of the combined growth constant
H = hydrodynamic (vortical) component of the combined growth constant
N = normal mode
0 = steady state

I. Introduction

WAVE motions in fluids originate from two sources: acoustics and hydrodynamics (vortex shedding). However, acoustic and hydrodynamic wave instabilities have been studied independently because many physical situations do not require coupling of the two distinctly different wave motions. For example, the hydrodynamic instability of water flowing underneath a sluice gate involves no acoustic wave motions. On the other hand, the acoustic instability of gases in the combustion chamber, without vortex shedding, does not involve hydrodynamic oscillations. Hydrodynamic instabilities are normally analyzed by solving the Orr-Sommerfeld equation,[1] whereas the acoustic instability is determined by means of the perturbed acoustic equation.[2-6] However, analytical solutions of hydrodynamic instabilities of other than incompressible parallel flows have not been studied in detail.

The coupling mechanism of both types of waves, acoustic and hydrodynamic, which allows them to interact together, is the subject of this study. Flandro[7] suggested that vortex shedding, due to the average flow past an obstruction, may provide another means of transferring energy to the acoustic field from the average flow. Culick and Magiawala[8] showed that acoustic modes in a tube may be excited by the average flow through two annular rings placed a suitable distance apart. Mason et al.[9] and Brown et al.,[10] conclude that vortex shedding may excite the fundamental longitudinal mode of the chamber. Despite these observations, rigorous mathematical foundations for the coupling of acoustic and vortical (hydrodynamic) waves are yet to be established.

Received April 27, 1982; revision received Feb. 25, 1986.

*Professor, Department of Mechanical Engineering.
†Graduate Research Assistant, Department of Mechanical Engineering.

Although it can be argued that the hydrodynamic instability may not occur in very high Reynolds numbers, the turbulent shear layer instabilities are found to be affected by various combinations of Strouhal and Reynolds numbers. The acoustic field may interact with vortex motions, known as the "feedback," thus resulting in the vortex generated sound.[11] Simple models, such as hyperbolic tangent velocity profiles for the shear layer[12,13] and temporal or spatial growth theories,[12-15] do not appear to be adequate for the interaction of acoustic and vortical oscillations in a rocket chamber in which such interaction must be permitted to occur everywhere in the domain.

In recent studies,[16] it has been shown that there is a possibility of the coexistence of acoustic and vortical frequencies which are, in fact, physically combined. For a given acoustic frequency, there exist many different vortical frequencies that may be excited. This phenomenon is typical of the segmented propellants with inhibitors in the Space Shuttle booster engine. At certain combinations of acoustic and vortical frequencies, the coupled acoustic and hydrodynamic wave oscillations may either cancel each other or amplify together. This observation is in contrast to the suggestion that vortex shedding simply leads to excitation of an acoustic mode. It is recognized that the hydrodynamically unstable waves exist independently of acoustically unstable waves and, indeed, they are capable of interacting together and emerging as a new state or combined stability or instability.

Our goal in this study, then, is to establish mathematical foundations for the coupling mechanism of acoustic and hydrodynamic wave oscillations. Toward this end, the total velocity is assumed to be the sum of the mean flow velocity and its deviations (oscillations), which consist of acoustic and vortical components. At any given time and space, these oscillations must be calculated relative to the mean flow velocity. In order to demonstrate the basic theory and strategies involved in this coupling mechanism, however, a very simple model with semianalytical solutions is first examined. For example, the Orr-Sommerfeld equation with a simple parabolic mean flow expression and hyperbolic tangent velocity profile for the free shear layer[14-17] in a parallel flow is utilized to calculate vortical frequencies or wavenumbers from which unsteady stream functions and, finally, vortically coupled acoustic growth constants are determined. With some insight into the coupling mechanism by means of this simple model, we then return to full-fledged governing equations for the multidimensional general flowfield in which the solution of the Orr-Sommerfeld equation is no longer valid. Toward this end, we must begin with the mean flow calculations by solving the Navier-Stokes system. Then, the natural frequencies and amplitudes of the acoustic field are calculated from the Helmholtz equation and vortical oscillaitons determined from the eigenvalue solution of the disturbance vorticity transport equation. With these data, growth constants for both acoustic and hydrodynamic oscillations can be calculated and stability boundaries constructed. All of the calculations are carried out using the finite element method.[17]

II. Vorticity-Coupled Acoustic Instability Integral

The basic governing equations for compressible viscous flow without particle distributions are represented as follows.

Continuity:

$$\frac{\partial \rho}{\partial t} + (\rho u_i)_{,i} = 0 \tag{1}$$

Momentum:

$$\frac{\partial}{\partial t}(\rho u_i) + (\rho u_i u_j)_{,j} + \frac{1}{\gamma} P_{,i} - \frac{1}{Re}\left(u_{i,jj} + \frac{1}{3} u_{j,ji}\right) = 0 \tag{2}$$

Energy:

$$\frac{\partial}{\partial t}(\rho T) - \frac{\gamma-1}{\gamma}\frac{\partial P}{\partial t} + (\rho u_i T)_{,i} - \frac{\gamma-1}{\gamma} u_i P_{,i} + \frac{\gamma-1}{Re}\left(\frac{2}{3} u_{i,i}u_{j,j} - u_{i,j}u_{j,i} - u_{i,j}u_{i,j}\right) = 0 \tag{3}$$

State:

$$P = \rho T \tag{4}$$

where the commas denote partial derivatives and the repeated indices imply summing. The following nondimensional quantities are used in the above equations:

$$u_i = \bar{\bar{u}}_i/a \qquad a = (\gamma P_0/\rho_0)^{1/2} \qquad P = \bar{\bar{P}}/P_0$$

$$T = c_p(\gamma-1)\bar{\bar{T}}/a^2 \qquad x_i = \bar{\bar{x}}_i/L \qquad t = a\bar{\bar{t}}/L$$

$$Re = \rho_0 a L/\mu \qquad \rho = \bar{\bar{\rho}}/\rho_0$$

where the double bars denote dimensional quantities.

Interactions between the acoustic and vortical oscillations can be introduced by superimposing the acoustic component upon the vortical component of the perturbed velocity in the form

$$u_i = \bar{u}_i + \epsilon(u' + u_i^*) \tag{5}$$

where the bars, primes, and asterisks indicate the mean flow and acoustic and vortical oscillations, respectively, and ϵ represents the perturbation parameter. On the other hand, the pressure and the density are given by

$$P = 1 + \epsilon P' \tag{6}$$

$$\rho = 1 + \epsilon \rho' \tag{7}$$

And, the vorticity field is given by

$$\xi_i = \bar{\xi}_i + \epsilon \xi_i^* \tag{8}$$

$$\bar{\xi}_i = \epsilon_{ijk}\bar{u}_{k,j} \tag{9}$$

$$\xi_i^* = \epsilon_{ijk}u_{k,j}^* \tag{10}$$

where ϵ_{ijk} is the permutation symbol. In view of Eqs. (1-10), it can be shown that the nonhomogeneous wave equation takes the following form:

$$P'_{,ii} - \frac{\partial^2 P'}{\partial t^2} = h \tag{11}$$

where

$$h = \bar{u}_i \frac{\partial P'_{,i}}{\partial t} + \gamma \frac{\partial P'}{\partial t}\bar{u}_{i,i} - \gamma[\bar{u}_{i,j}(u_j' + u_j^*) + (u_{i,j}' + u_{i,j}^*)\bar{u}_j]_{,i} + \frac{\gamma}{Re}\left[(u_i^* + u_i')_{,jji} + \frac{1}{3}(u_j^* + u_j')_{,jii}\right] + \frac{2\gamma(\gamma-1)}{Re}\frac{\partial}{\partial t}\left[\frac{2}{3}\bar{u}_{i,i}(u_j^* + u_j')_{,j} - \bar{u}_{i,j}(u_j^* + u_j')_{,i} - \bar{u}_{j,i}(u_j^* + u_j')_{,i}\right] \tag{12}$$

The boundary condition can be obtained from the momentum equation by constructing a dot product with the normal

vector,

$$-P'_{,i}n_i = f \tag{13}$$

where

$$f = \gamma\left\{\frac{\partial u_i'}{\partial t} + \bar{u}_{i,j}(u_j' + u_j^*) + (u_{i,j}' + u_{i,j}^*)\bar{u}_j - \frac{1}{Re}\left[(u_i^* + u_i')_{,jj} + \frac{1}{3}(u_j^* + u_j')_{,ji}\right]\right\}n_i \tag{14}$$

The oscillatory motions in both acoustic and vortical fields are modeled by

$$P' = \hat{P}e^{ikt} \tag{15}$$

$$u_i' = \hat{u}_i' e^{ikt} \qquad u_i^* = \hat{u}_i^* e^{ikt} \tag{16}$$

$$\xi_i^* = \hat{\xi}_i^* e^{ikt} \tag{17}$$

where k is the complex dimensionless frequency given by

$$k = \omega - i\alpha \tag{18}$$

Here, ω is the dimensionless frequency, the imaginary part α is known as the growth constant, and k^* is the complex vortical wavenumber.

Substituting Eqs. (15–18) into the wave equation, we arrive at the nonhomogeneous Helmholtz equation,

$$\hat{P}_{,ii} + k^2\hat{P} = \hat{h} \tag{19}$$

and the boundary condition,

$$-\hat{P}_{,i}n_i = \hat{f} \tag{20}$$

The nonhomogeneous terms $\hat{h}$ and $\hat{f}$ are given by

$$\hat{h} = ik\bar{u}_i\hat{P}_{,i} + ik\gamma\bar{u}_{i,i}\hat{P} - \gamma[\bar{u}_{i,j}(\hat{u}_j' + u_j^*) + (\hat{u}_{i,j}' + \hat{u}_{i,j}^*)\bar{u}_j]_{,i} + \gamma/Re[(\hat{u}_i^* + \hat{u}_i')_{,jji} + \tfrac{1}{3}(\hat{u}_j^* + \hat{u}_j')_{,jii}] + [2ik\gamma(\gamma-1)]/Re[\tfrac{2}{3}\bar{u}_{i,i}(\hat{u}_j^* + \hat{u}_j')_{,j} - \bar{u}_{i,j}(\hat{u}_j^* + \hat{u}_j')_{,i} - \bar{u}_{j,i}(\hat{u}_j^* + \hat{u}_j')_{,i}] \tag{21}$$

and

$$\hat{f} = \gamma\{ik\hat{u}_i' + \bar{u}_{i,j}(\hat{u}_j' + \hat{u}_j^*) + (\hat{u}_{i,j}' + \hat{u}_{i,j}^*)\bar{u}_j - 1/Re[(\hat{u}_i^* + \hat{u}_i')_{,jj} + \tfrac{1}{3}(\hat{u}_j^* + \hat{u}_j')_{,ji}]\}n_i \tag{22}$$

Making use of the Green's function integral,[18] it can be shown that

$$(k^2 - k_N^2)E_N^2 = \int_\Omega \hat{h}\hat{P}_N d\Omega + \int_\Gamma \hat{f}\hat{P}_N d\Gamma \tag{23}$$

where the unperturbed mode shape $\hat{P}_N$ and its frequency k_N are determined from the classical acoustic problem,

$$\hat{P}_{N,ii} + k^2\hat{P}_N = 0 \tag{24}$$

$$\hat{P}_{N,i}n_i = 0 \tag{25}$$

and E_N is given by

$$E_N^2 = \int_\Omega \hat{P}_N^2 d\Omega \tag{26}$$

At this point, an important remark is in order. A close examination of Eq. (23) reveals that the domain integral on the right-hand side of Eq. (23) contains the terms from the momentum equation that were differentiated once. Thus, these terms must be integrated once by parts to produce an acoustic boundary condition. The resulting domain integral represents the functional space equivalent to the mean flow characterized by the Navier-Stokes system. This imples that an additional integration by parts must be carried out such that the familiar Neumann boundary conditions may be brought to the surface. The boundary integrals arrived at in this manner account for the stress and/or the pressure boundary conditions by means of velocity gradients. Such Neumann boundary conditions stem from the convective and viscous terms.

In view of these requirements, the resulting expression upon integration by parts twice of Eq. (23) takes the form

$$(k^2 - k_N^2)E_N^2 = i\gamma k_N\int_\Gamma \hat{u}_i'\hat{P}_N n_i d\Gamma + ik_N(\gamma+1)\int_\Gamma \bar{u}_i\hat{P}_N^2 n_i d\Gamma - ik_N\int_\Omega \bar{u}_{i,i}\hat{P}_N^2 d\Omega - ik_N(2\gamma+1)\int_\Omega \bar{u}_i\hat{P}_N\hat{P}_{N,i}d\Omega + \gamma\int_\Gamma [\bar{u}_i(\hat{u}_j^* + \hat{u}_j') + (\hat{u}_i^* + \hat{u}_i')\bar{u}_j]\hat{P}_{N,i}n_j d\Gamma - \gamma\int_\Omega \{[\bar{u}_i(\hat{u}_j^* + \hat{u}_j')_{,j} + (\hat{u}_i^* + \hat{u}_i')\bar{u}_{j,j}]\hat{P}_{N,i} + [\bar{u}_i(\hat{u}_j^* + \hat{u}_j') + (\hat{u}_i^* + \hat{u}_i')\bar{u}_j]\hat{P}_{N,ij}\}d\Omega - \frac{\gamma}{Re}\int_\Gamma\left[(\hat{u}_i^* + \hat{u}_i')_{,j}\hat{P}_{N,i}n_j + \frac{1}{3}(\hat{u}_j^* + \hat{u}_j')_{,j}\hat{P}_{N,i}n_i\right]d\Gamma + \frac{\gamma}{Re}\int_\Omega\left[(\hat{u}_i^* + \hat{u}_i')_{,j}\hat{P}_{N,ij} + \frac{1}{3}(\hat{u}_j^* + \hat{u}_j')_{,j}\hat{P}_{N,ii}\right]d\Omega + \frac{2ik_N\gamma(\gamma-1)}{Re}\int_\Omega\left[\frac{2}{3}\bar{u}_{i,i}(\hat{u}_j^* + \hat{u}_j')_{,j} - \bar{u}_{i,j}(\hat{u}_j^* + \hat{u}_j')_{,i} - \bar{u}_{j,i}(\hat{u}_j^* + \hat{u}_j')_{,i}\right]\hat{P}_N d\Omega \tag{27}$$

Squaring both sides of Eq. (18) and assuming that

$$\omega \simeq \omega_N \simeq k_N \tag{28}$$

for $\alpha \simeq 0$, we obtain

$$k^2 - k_N^2 = -i2\alpha k_N + \alpha^2 \tag{29}$$

Since $\alpha^2 \ll |2\alpha k_N|$ from the condition set by Eq. (28), it is now possible to solve for the growth rate α by equating the imaginary parts between Eqs. (27) and (29),

$$\alpha = -\frac{1}{2E_N^2}\Bigg[\underbrace{\int_\Gamma\left\{\gamma\hat{u}_i'^{(R)}\hat{P}_N n_i + (\gamma+1)\bar{u}_i\hat{P}_N^2 n_i\right.}_{\text{A}} + \underbrace{\frac{\gamma}{k_N}[\bar{u}_i(\hat{u}_j^* + \hat{u}_j')^{(I)} + (\hat{u}_i^* + \hat{u}_i')^{(I)}\bar{u}_j]\hat{P}_{N,i}n_j}_{\text{B}} \underbrace{\left. - \frac{\gamma}{k_N Re}\left[(\hat{u}_i^* + \hat{u}_i')_{,j}^{(I)}\hat{P}_{N,i}n_j + \frac{1}{3}(\hat{u}_j^* + \hat{u}_j')_{,j}^{(I)}\hat{P}_{N,i}n_i\right]\right\}d\Gamma}_{\text{C}}$$

$$+\int_\Omega \underbrace{\{-\bar{u}_{i,i}\hat{P}_N^2-(2\gamma+1)\bar{u}_i\hat{P}_N\hat{P}_{N,i}}_{D}$$

$$\underbrace{-\frac{\gamma}{k_N}[\bar{u}_i(\hat{u}_j^*+\hat{u}_j')^{(I)}_{,j}+(\hat{u}_i^*+\hat{u}_i')^{(I)}\bar{u}_{j,j}]\hat{P}_{N,i}}_{E}$$

$$\underbrace{-\frac{\gamma}{k_N}[\bar{u}_i(\hat{u}_j^*+\hat{u}_j')^{(I)}+(\hat{u}_i^*+\hat{u}_i')^{(I)}\bar{u}_j]\hat{P}_{N,ij}}_{E}$$

$$\underbrace{+\frac{\gamma}{k_N Re}\left[(\hat{u}_i^*+\hat{u}_i')^{(I)}_{,j}\hat{P}_{N,ij}+\frac{1}{3}(\hat{u}_j^*+\hat{u}_j')^{(I)}_{,j}\hat{P}_{N,ii}\right]}_{F}$$

$$\underbrace{+\frac{2\gamma(\gamma-1)}{Re}\left[\frac{2}{3}\bar{u}_{i,i}(\hat{u}_j^*+\hat{u}_j')^{(R)}_{,j}-\bar{u}_{i,j}(\hat{u}_j^*+\hat{u}_j')^{(R)}_{,i}\right.}_{G}$$

$$\underbrace{\left.-\bar{u}_{j,i}(\hat{u}_j^*+\hat{u}_j')^{(R)}_{,i}\right]\hat{P}_N\}d\Omega\Big]}_{G} \tag{30}$$

where the superscripts (R) and (I) refer to the real and the imaginary parts, respectively.

The normal velocity at the surface can be expressed in terms of the admittance, $A=A^{(R)}+iA^{(I)}$, and the mean flow Mach number $\bar{M}$ such that

$$\hat{u}_i' n_i=(\hat{u}_i'^{(R)}+i\hat{u}_i'^{(I)})n_i=\bar{M}A\hat{P}_N/\gamma \tag{31}$$

whereas the acoustic fluctuation velocity in the domain is given by

$$\hat{u}_i'=\frac{i}{k_N\gamma}\hat{P}_{N,i} \tag{32}$$

For the purpose of investigating the coupling mechanism of acoustic and hydrodynamic instabilities, it is convenient to separate Eq. (30) into two parts,

$$\alpha=\alpha_A+\alpha_H \tag{33}$$

where α_A and α_H refer to the acoustic growth constant and the acoustically coupled vortical growth constants, respectively. Then

$$\alpha_A=-\frac{1}{2E_N^2}\underbrace{\{-A_b^{(R)}\bar{M}_b\int_{\Gamma_b}\hat{P}_N^2 d\Gamma_b+A_n^{(R)}\bar{M}_n\int_{\Gamma_n}\hat{P}_N^2 d\Gamma_n}_{A}$$

$$\underbrace{-(\gamma+1)\int_\Gamma \bar{u}_i\hat{P}_N^2 n_i d\Gamma}_{A}$$

$$\underbrace{+\frac{1}{k_N^2}\int_\Gamma(\bar{u}_j\hat{P}_{N,i}\hat{P}_{N,i}n_j+\bar{u}_i\hat{P}_{N,i}\hat{P}_{N,j}n_j)d\Gamma}_{B}$$

$$\underbrace{-\frac{1}{k_N^2 Re}\int_\Gamma\left(\hat{P}_{N,i}\hat{P}_{N,ij}n_j+\frac{1}{3}\hat{P}_{N,jj}\hat{P}_{N,i}n_i\right)d\Gamma}_{C}$$

$$+\int_\Omega\underbrace{\left[-\bar{u}_{i,i}\hat{P}_N^2-(2\gamma+1)\bar{u}_i\hat{P}_N\hat{P}_{N,i}\right.}_{D}$$

$$\underbrace{-\frac{1}{k_N^2}(\bar{u}_i\hat{P}_{N,jj}\hat{P}_{N,i}+\hat{u}_{j,j}\hat{P}_{N,i}\hat{P}_{N,i}+\bar{u}_i\hat{P}_{N,j}\hat{P}_{N,ij}}_{E}$$

$$\underbrace{\left.+\bar{u}_j\hat{P}_{N,i}\hat{P}_{N,ij}\right)}_{E}$$

$$\underbrace{\left.+\frac{1}{k_N^2 Re}\left(\hat{P}_{N,ij}\hat{P}_{N,ij}+\frac{1}{3}\hat{P}_{N,ii}\hat{P}_{N,jj}\right)\right]d\Omega\Big\}}_{F} \tag{34}$$

$$\alpha_H=-\frac{1}{2E_N^2}\underbrace{\Big\{\int_\Gamma\left[\frac{\gamma}{k_N}(\bar{u}_j\hat{u}_i^{*(I)}+\hat{u}_j^{*(I)}\bar{u}_i)\hat{P}_{N,i}n_j\right.}_{B}$$

$$\underbrace{\left.-\frac{\gamma}{k_N Re}\left(\hat{u}_{i,j}^{*(I)}\hat{P}_{N,i}n_j+\frac{1}{3}\hat{u}_{j,j}^{*(I)}\hat{P}_{N,i}n_i\right)\right]d\Gamma}_{C}$$

$$+\int_\Omega\underbrace{\left[-\frac{\gamma}{k_N}(\bar{u}_i\hat{u}_{j,j}^{*(I)}\hat{P}_{N,i}+\bar{u}_{j,j}\hat{u}_i^{*(I)}\hat{P}_{N,i}+\bar{u}_i\hat{u}_j^{*(I)}\hat{P}_{N,ij}\right.}_{E}$$

$$\underbrace{\left.+\bar{u}_j\hat{u}_i^{*(I)}\hat{P}_{N,ij}\right)}_{E}$$

$$\underbrace{+\frac{\gamma}{k_N Re}\left(\hat{u}_{i,j}^{*(I)}\hat{P}_{N,ij}+\frac{1}{3}\hat{u}_{j,j}^{*(I)}\hat{P}_{N,ii}\right)}_{F}$$

$$\underbrace{\left.+\frac{2\gamma(\gamma-1)}{Re}\left(\frac{2}{3}\bar{u}_{i,i}\hat{u}_{j,j}^{*(R)}-\bar{u}_{i,j}\hat{u}_{j,i}^{*(R)}-\bar{u}_{j,i}\hat{u}_{j,i}^{*(R)}\right)\hat{P}_N\right]d\Omega\Big\}}_{G} \tag{35}$$

The physical implications of the individual contributions in the stability integral above may be summarized as follows:

A) Surface combustion (acoustic boundary conditions on burning surface Γ_b and nozzle surface Γ_n, which arise directly from the first term in Eq. (22), and additional acoustic boundary conditions as a result of the first integration by parts of the first two terms in Eq. (21) associated with the mean flow velocity).

B) Surface convection (flow turning or Neumann boundary conditions due to convection).

C) Surface viscous damping (Neumann boundary conditions due to surface traction).

D) Combustion into domain.

E) Convection into domain.

F) Momentum viscous damping in domain.

G) Dissipation energy in domain.

Note that the first term of the boundary integrals, designated as B in Eq. (34),

$$-\frac{1}{2E_N^2}\int_\Gamma\frac{1}{k_N}\bar{u}_j\hat{P}_{N,i}\hat{P}_{N,i}n_j d\Gamma$$

is seen to be identical to the three-dimensional equivalent of the one-dimensional flow turning term which appeared in Culick,[5] but which did not arise in due course of mathematical derivations for the three-dimensional case.[6] To reconstruct the present results in terms of the same dimensions and notations as in Ref 6, we set

$$k_N = a\bar{k}_N, \quad P = \bar{P}/P_0, \quad u = \bar{u}/a, \quad a = (\gamma P_0/\bar{\rho})^{1/2}$$

Substituting these relations and Eq. (31) into Eq. (34), collecting the first two terms of A and the flow turning term, and rewriting in the same form as Eq. (27), we obtain

$$(k^2 - k_N^2)E_N^2 = i\bar{\rho}ak_N \int_\Gamma \left(\hat{u}'\hat{P}_N + \frac{\hat{P}_N^2}{\bar{\rho}a^2}\bar{u}\right)\cdot n\,d\Gamma + i\frac{1}{\bar{\rho}ak_N}\int_\Gamma (\nabla\hat{P}_N)^2\bar{\rho}\bar{u}\cdot n\,d\Gamma \tag{36}$$

It is seen that $\bar{\rho}\bar{u}\cdot n$ is equivalent to $\bar{M}_b\delta_\parallel$ in terms of the notations used in Ref. 6. Notice that Eq. (36) is the same as Eq. (4.14) in Ref. 6, neglecting the particle distribution of the two-phase flow.

To describe the vorticity field, we return to Eq. (1b). Taking a curl of this equation, we obtain the vortical diffusion equation,

$$\frac{\partial\xi}{\partial t} - \nabla\times(u\times\xi) - \frac{1}{Re}\nabla^2\xi = 0 \tag{37}$$

Collecting the terms of $\mathcal{O}(\epsilon)$,

$$\frac{\partial\xi^*}{\partial t} - \nabla\times(\bar{u}\times\xi^* + u'\times\bar{\xi} + u^*\times\bar{\xi}) - \frac{1}{Re}\nabla^2\xi^* = 0 \tag{38}$$

Introducing Eqs. (16) and (17), we obtain

$$(i/Re)\nabla^2\hat{\xi}^* + k\hat{\xi}^* - \hat{H} = 0 \tag{39}$$

where

$$\hat{H} = i\nabla\times(\bar{u}\times\hat{\xi}^* + \hat{u}'\times\bar{\xi} + \hat{u}^*\times\bar{\xi}] \tag{40}$$

subject to the boundary condition

$$(i/Re)(n\cdot\nabla)\hat{\xi}^* = -\hat{F} \tag{41}$$

To calculate the vortical frequencies k_N^* and mode shapes $\hat{\xi}_N^*$, we return to Eq. (39). Noting that

$$\hat{\xi}^* = \nabla\times u^* \tag{42}$$

$$\xi = \nabla\times\bar{u} \tag{43}$$

we obtain

$$(i/Re)\nabla^2(\nabla\times\hat{u}^*) + k^*(\nabla\times\hat{u}^*) - \nabla\times[\bar{u}\times(\nabla\times u^*) + (i/k_N\gamma)\nabla\hat{P}_N\times(\nabla\times\bar{u}) + \hat{u}^*\times(\nabla\times\bar{u})] = 0 \tag{44}$$

in which $\hat{P}_N$ and $\bar{u}$ are now known quantities. For two-dimensional flow without acoustics in which the vorticity in the x_1-x_2 plane can be defined as

$$\hat{\xi}^* = -\frac{\partial^2\hat{\psi}^*}{\partial x_i\partial x_i}, \quad \bar{\xi} = -\frac{\partial^2\bar{\psi}}{\partial x_i\partial x_i}, \quad \hat{u}_i^* = \epsilon_{ij}\frac{\partial\hat{\psi}^*}{\partial x_j} \tag{45}$$

the characteristic equation (44) takes the form

$$\frac{\partial}{\partial t}\left(\frac{\partial^2\psi^*}{\partial x_i\partial x_i}\right) + \frac{\partial}{\partial x_j}\left(\epsilon_{mn}\frac{\partial\bar{u}_n}{\partial x_m}\right)\xi_{jk}\frac{\partial\psi^*}{\partial x_k} - \frac{\partial}{\partial x_j}\left(\frac{\partial^2\psi^*}{\partial x_i\partial x_i}\right)\bar{u}_j - \frac{1}{Re}\frac{\partial^4\psi^*}{\partial x_i\partial x_j\partial x_i\partial x_j} = 0 \tag{46}$$

Using the exponential oscillations of $\hat{\psi}^*$ in the form

$$\hat{\psi}^* = \phi e^{ikt} \tag{47}$$

we obtain

$$ik^*\frac{\partial^2\phi}{\partial x_i\partial x_i} - \frac{\partial}{\partial x_j}\left(\epsilon_{mn}\frac{\partial\bar{u}_n}{\partial x_m}\right)\epsilon_{jk}\frac{\partial\phi}{\partial x_k} + \frac{\partial}{\partial x_j}\left(\frac{\partial^2\phi}{\partial x_i\partial x_i}\right)\bar{u}_j - \frac{1}{Re}\frac{\partial^4\phi}{\partial x_i\partial x_j\partial x_i\partial x_j} = 0 \tag{48}$$

It is interesting to note that the above equation reduces to the Orr-Sommerfeld equation for the parallel flow [$\bar{u}_2 = 0$, $\bar{u} = \bar{u}(y)$, $\phi(x,y) = \phi(y)e^{i\bar{k}x}$] in the form

$$(\bar{u} - c)(\phi'' - \bar{k}^2\phi) - u''\phi = -(i/\bar{k}Re)(\phi'''' - 2\bar{k}^2\phi'' + \bar{k}^4\phi) \tag{49}$$

where $c = c^{(R)} + ic^{(I)}$, the real part being the phase velocity and the imaginary part being the measure of amplification of disturbance (or equivalent to growth constant), and $\bar{k}$ is the vortical wavenumber. Note also that the relations $c = \omega^*/\bar{k}$ and $\omega^* = -k^*$ are used in Eq. (48) to obtain Eq. (49). From this development, it is clearly seen that the Orr-Sommerfeld equation is a special case of the general form of the vortical instability equation in multidimensions given in Eq. (48).

III. Physical and Computational Models

Simple Model

The mathematics and associated physics presented above are extremely complex. Anticipating that computations and results are also equally complicated, it is advisable to demonstrate a simpler model (Fig. 1a) in order to illustrate the key feature. Toward this end, we choose to retain only those terms essential to the coupling mechanism of the acoustic and vortical oscillations. Thus, we modify Eqs. (21) and (22) as

$$\hat{h} = -\gamma(\bar{u}_{i,j}\hat{u}_j^{*(I)} + \hat{u}_{i,j}^{*(I)}\bar{u}_j)_{,i} \tag{50}$$

$$\hat{f} = \gamma(\bar{u}_{i,j}\hat{u}_j^{*(I)} + \hat{u}_{i,j}^{*(I)}\bar{u}_j)n_i \tag{51}$$

in which only the mean flow and vortical component of velocity, which are to be combined with the Helmholtz equation, are retained. This assumption is logical, since the effect of viscosity may be neglected and the absence of the first two terms and the acoustic component of the velocity in Eqs. (21) and (22) will not invalidate the coupling mechanism embedded in Eq. (33). This simplification allows Eq. (35) to be written as

$$\alpha = \frac{\gamma}{2k_N E_N^2}\int_0^L\int_{-1}^1\left(\frac{d\bar{u}}{dy}\hat{v}^{*(I)} + \frac{\partial\hat{u}^{*(I)}}{\partial x}\bar{u}\right)\frac{d\hat{P}_N}{dx}\,dy\,dx \tag{52}$$

in which a parabolic mean flow is assumed (Fig. 1a),

$$\bar{u}(y) = 1 - y^2 \tag{53}$$

Assuming that

$$\hat{P}_N = \cos k_N x, \quad k_N = \pi n/(L+h), \quad n = 0,1,2,... \tag{54}$$

and

$$\psi^*(x,y,t) = \phi(y) e^{i\bar{k}(x-ct)} \tag{55}$$

the growth constant α in Eq. (52) takes the form

$$\alpha = \frac{\bar{k}\gamma}{E_N^2(\bar{k}^2 - k_N^2)} \Big\{ [(\bar{k}+k_N)\cos(\bar{k}-k_N)L + (\bar{k}-k_N)\cos(\bar{k}+k_N)L - 1] \int_{-1}^{1} y\phi^{(R)}(y)\mathrm{d}y + [(\bar{k}+k_N)\sin(\bar{k}-k_N)L - (\bar{k}-k_N)\sin(\bar{k}+k_N)L] \int_{-1}^{1} y\phi^{(I)}(y)\mathrm{d}y \Big\} \tag{56}$$

where

$$E_N^2 = \int_{-h}^{L} \cos^2 k_N x \mathrm{d}x \tag{57}$$

To obtain real and imaginary parts of stream functions, $\phi^{(R)}(y)$ and $\phi^{(I)}(y)$, we invoke the Orr-Sommerfeld equation (49) subject to the boundary condition,

$$\phi(\pm 1) = \phi'(\pm 1) = 0 \tag{58}$$

The solution of this equation is combined with Eq. (55) and substituted into

$$\psi(x,y,t) = \bar{\psi}(y) + \epsilon\psi^*(x,y,t) \tag{59a}$$

or

$$\psi(x,y,t) = y - \tfrac{1}{3}y^3 + \epsilon\{\phi^{(R)}(y)\cos[\bar{k}(x-ct)] - \phi^{(I)}(y)\sin[\bar{k}(x-ct)]\} \tag{59b}$$

This will allow prediction of various modes of streamlines indicating stable and unstable vortex oscillations. Subsequently, the growth constants vs Reynolds numbers or Strouhal numbers can be obtained from Eq. (56).

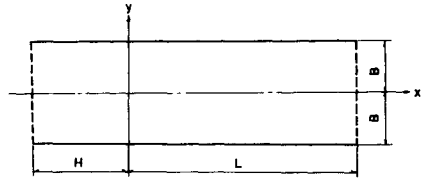

a) Simple model (two-dimensional): $B=1.0$, $H=4.0$, $L=10.0$, mean velocity $\bar{u}=1-y^2$, vortical component of velocity u_i^* calculated from Orr-Sommerfeld equation.

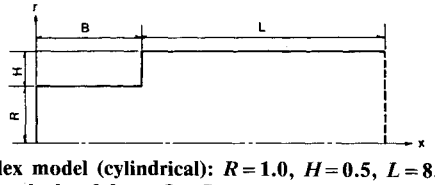

b) Complex model (cylindrical): $R=1.0$, $H=0.5$, $L=8.0$, $B=2.0$. Case 1: u_i^* calculated from Orr-Sommerfeld equation for the region of flow separation at the step and subsequent free shear layers with the hyperbolic tangent mean flow velocity (shear layer as determined by $\delta_0 = f(R\sqrt{Re})$). Case 2: u_i^* calculated from general vortical disturbance equation (48) using finite elements.

Fig. 1 Various computational models.

Complex Model

The simple model given in the previous section [Eq. (56)] is useful in demonstrating the basic idea of coupling the acoustic and vortical oscillations to calculate the combined growth constants. The approximations imposed in Eqs. (50-59) and Fig. 1a are, however, too restrictive in view of real-world situations such as those found in rocket motor combustion chambers. To relax the restrictions, the fully nonhomogeneous Helmholtz equation (21) is restored, along with the expressions for the growth constants α_A [Eq. (34)] and α_H [Eq. (35)]. Arbitrary geometries, such as the stepped cylinder shown in Fig. 1b, require the mean flow calculation to be performed numerically.

The unstable vortical oscillations are calculated from the general vortical disturbance equation (48) with a numerically computed mean flowfield. For the purpose of comparison, we shall demonstrate the use of the Orr-Sommerfeld equation within the free shear layer behind the separation point, using the analytically assumed mean velocity distribution. With the Orr-Sommerfeld equation, the thickness of the free shear layer is expressed as a function of the diameter and Reynolds number,[15]

$$\delta_0 = f(R/\sqrt{Re}) \tag{60}$$

where R is the characteristic dimension of the chamber. Furthermore, the boundary condition for the Orr-Sommerfeld equation (49) is

$$\phi(\pm\infty) = \phi'(\pm\infty) = 0 \tag{61}$$

and the freestream mean velocity in the free shear layer is given by the hyperbolic tangent velocity profile,[12-15]

$$\bar{u} = \tfrac{1}{2}(1 + \tanh y) \tag{62}$$

This approximation is deliberately chosen for two reasons. First of all, this approach has been accepted for most of the vortical instability problems with favorable correlations with experimental data.[15] Second, it is felt that an analytical simulation such as Eq. (62) is convenient to demonstrate the essential theory leading to the expression for the acoustically coupled vortical instability growth constant [Eq. (35)]. There are two approaches to the vortical mode analysis by the Orr-Sommerfeld equation, i.e., temporal and spatial growth concepts of disturbance. The limitations of these approaches in the acoustic-vortical coupling will be discussed in Sec. IV. On the other hand, the rigorous approach is clearly the solution of the general vortical disturbance equation (48). In this case, there are no limitations on the thickness of the free shear layer and the no-slip boundary conditions at the solid surface can be used. The merits of this model are as follows: 1) the unstable vortical oscillations are based on the practical mean velocity fields that depend on the actual geometry and Reynolds number, 2) there are no limitations as to the establishment of vortically unstable regions, and 3) the vortical modes can be obtained as they appear in the finite dimensions.

Thus, in the proposed model, the Navier-Stokes mean flow calculations [Eqs. (1-4)], acoustic eigenvalue analysis [Eqs. (24) and (25)], and vortical mode analysis [Eqs. (48) and (49)] are performed for the entire domain (Fig. 1b). These results are then entered in Eqs. (34) and (35) to compute the acoustic and vortical instability growth constants for various combinations of acoustic and vortical frequencies. Vortical frequencies are converted to Strouhal numbers to display the results for various Reynolds numbers.

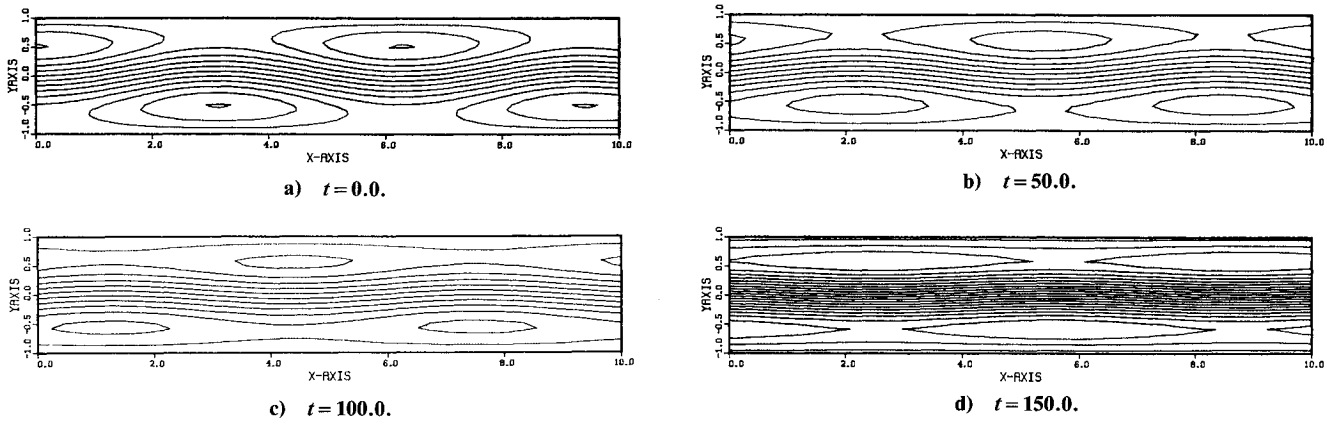

a) $t=0.0$. b) $t=50.0$. c) $t=100.0$. d) $t=150.0$.

Fig. 2 Simple model streamline distributions in stable vortical modes [the negative imaginary part of eigenvalue solutions in Orr-Sommerfeld equation defines stable motion, streamlines calculated from Eq. (59)], $Re=10^5$, $\bar{k}=1.0$, 24 Hermite polynomial linear finite elements, flow tends to be laminar as $t\to\infty$.

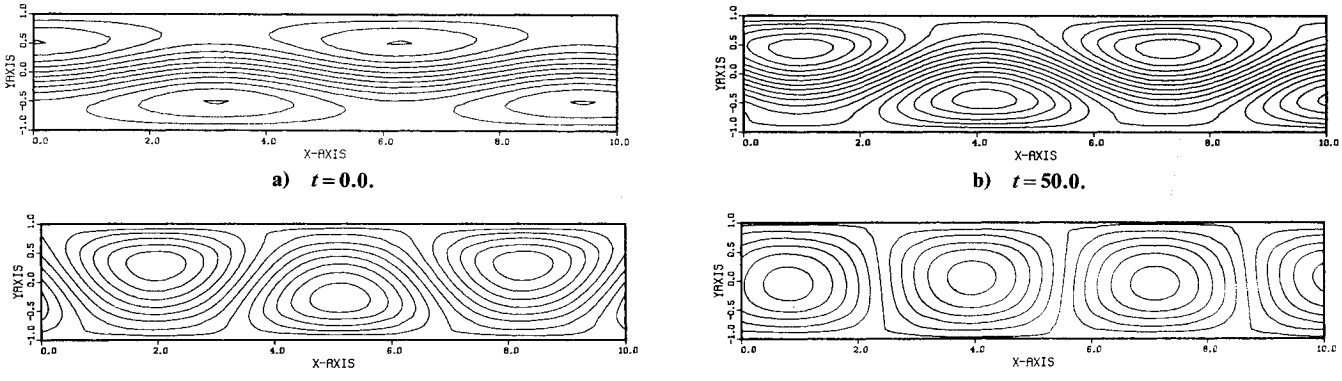

a) $t=0.0$. b) $t=50.0$. c) $t=100.0$. d) $t=150.0$.

Fig. 3 Simple model streamline distributions in unstable vortical modes [the positive imaginary part of eigenvalue solutions in Orr-Sommerfeld equation defines unstable motion, streamlines calculated from Eq. (59)], $Re=10^4$, $\bar{k}=1.0$, 24 Hermite polynomial linear finite elements, flow tends to be turbulent and numerical breakdown occurs as $t\to\infty$.

Finite Element Analysis

All numerical analyses are performed using the finite element method. The differential equations and their finite element analogs are as follows.

Simple Model

The Orr-Sommerfeld equation (49) is converted into the finite element analog by constructing the Galerkin integral and integrating by parts twice in order to bring the fourth-order differential equation into a weak form. The resulting weak form contains second-order derivatives that would require at least second-degree polynomials as trial and test functions. The Hermit polynomial Φ_α is ideal for this situation and the resulting finite element eigenvalue problem takes the form,

$$|K_{\alpha\beta}-cM_{\alpha\beta}|=0 \tag{63}$$

where

$$K_{\alpha\beta}=\int_\delta \left[(\bar{u}\Phi_\alpha'+\Phi_\alpha\bar{u}')\Phi_\beta'+a^2\Phi_\alpha\Phi_\beta\bar{u} -\frac{i}{aRe}(\Phi_\alpha''\Phi_\beta''+2a^2\Phi_\alpha'\Phi_\beta'+a^4\Phi_\alpha\Phi_\beta)\right]dy \tag{64}$$

$$M_{\alpha\beta}=\int_\delta (\Phi_\alpha'\Phi_\beta'+a^2\Phi_\alpha\Phi_\beta)dy \tag{65}$$

Here, the prime denotes the derivative with respect to the y direction and the mean flow velocity $\bar{u}$ is given by Eq. (53). For a given vortical wavenumber $\bar{k}$, we calculate the speed of propagation c (indicative of frequency and the Strouhal number) from Eq. (63), and the corresponding unstable vortical component of stream function amplitudes by means of Eq. (59). Finally, using the analytical form of acoustic frequencies and amplitudes [Eq. (54)], the acoustically coupled vortical instability growth constants are calculated from Eq. (56) with the finite element analog cast in the form

$$\alpha=\int_{-1}^{1}F(y)dy=\sum_{i=1}^{n}w_iF(y_i) \tag{66}$$

which represents the one-dimensional Gaussian quadrature integration.

Complex Model

In this model, we first solve the Navier-Stokes system to obtain the mean flowfield of the entire domain (Fig. 1b). For simplicity, in the present paper, unsteady, isothermal, incompressible flow is assumed. Combining the continuity with the momentum equation, the finite element analog takes the form,

$$A_{\alpha\beta}\dot{u}_{\beta i}+B_{\alpha\beta j\gamma}u_{\beta j}u_{\gamma i}+(1/Re)C_{\alpha\beta}u_{\beta i}=-(1/\gamma)D_{\alpha\beta i}P_\beta \tag{67}$$

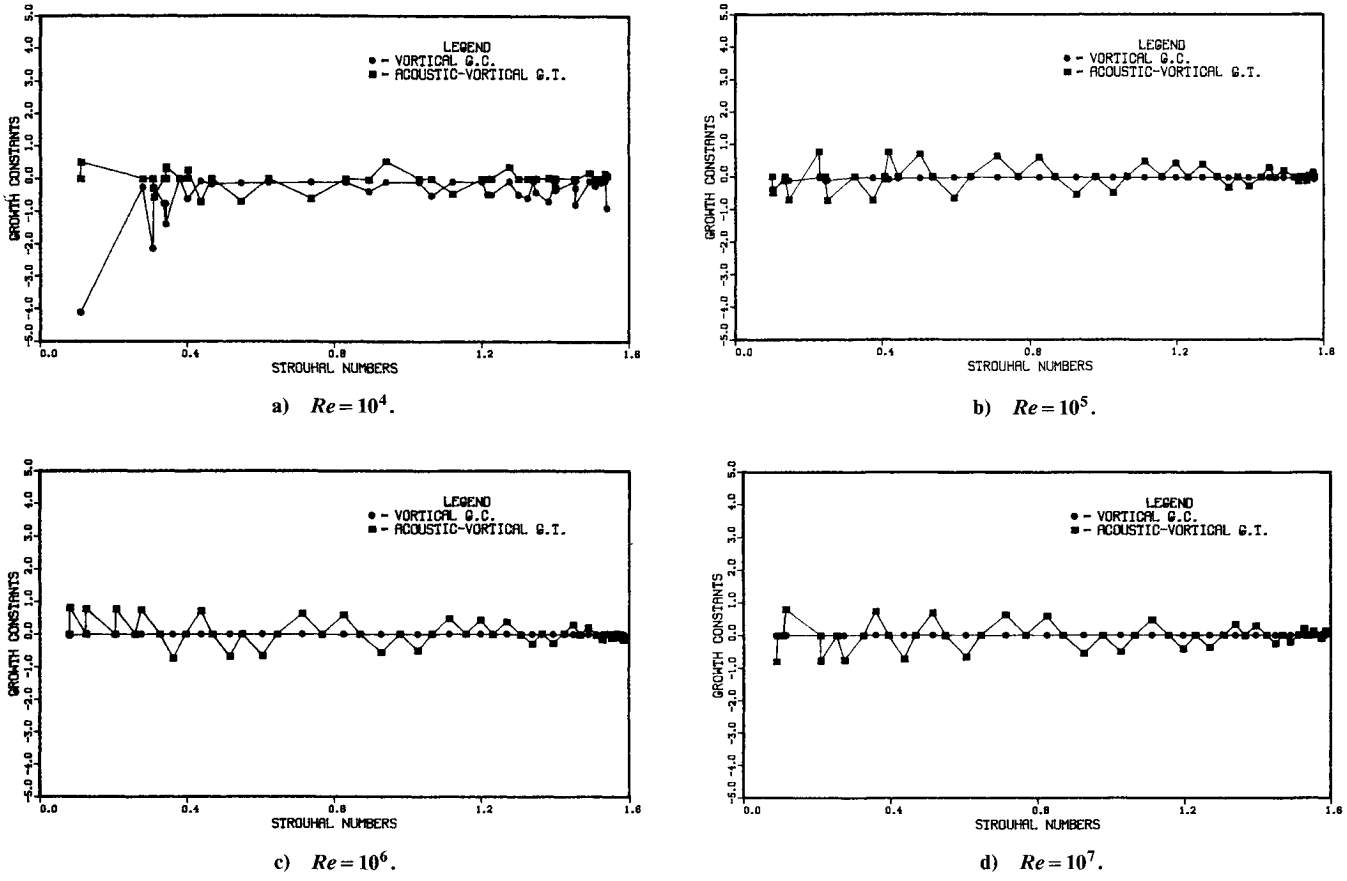

a) $Re = 10^4$. b) $Re = 10^5$.

c) $Re = 10^6$. d) $Re = 10^7$.

Fig. 4 Growth constants vs Strouhal numbers in simple model, $\bar{k} = 1.0$, first acoustic mode. Vortical growth constants calculated from the imaginary parts of the eigenvalues of Orr-Sommerfeld equation, acoustic-vortical growth constants calculated from the semianalytic form [Eq. (56)], pronounced amplification of growth constants at low Strouhal number and high Reynolds number when vortical disturbances are coupled with acoustic disturbances.

where

$$A_{\alpha\beta} = \int_\Omega \Phi_\alpha \Phi_\beta d\Omega \tag{68a}$$

$$B_{\alpha\beta j\gamma} = \int_\Omega \Phi_\alpha \Phi_{\beta,j} \Phi_\gamma d\Omega \tag{68b}$$

$$C_{\alpha\beta} = \int_\Omega \Phi_{\alpha,i} \Phi_{\beta,i} d\Omega \tag{68c}$$

$$D_{\alpha\beta i} = \int_\Omega \Phi_\alpha \Phi_{\beta,i} d\Omega \tag{68d}$$

The trial and test functions Φ_α are chosen as four-sided linear isoparametric elements. Although various solution strategies are available to solve Eq. (67), we employ linearization and sequential corrections in the present paper. The calculated velocities are designated as $\bar{u}_i$, as shown in Eqs. (34) and (35).

The next step is to calculate the frequency and amplitude of the vortical component of the velocity u_i^*, which can be calculated from either the Orr-Sommerfeld or the general vortical disturbance equation. In the Orr-Sommerfeld equation, the shear layer thickness δ_0 is taken as $H/3$, with the total positive and negative dimension being $2H/3$ for computational purposes. In the case of temporal growth of the disturbance, the finite element equation is represented by the same form as Eqs. (63-65). In the case of spatial growth of the disturbance and because of nonlinearity in the eigenvalue analysis, the fourth-order Runge-Kutta method is used for the inviscid case with the same procedure followed by Michalke[14] for comparison and verification.

In the general vortical disturbance equation, the finite element equation has the form

$$|H_{\alpha\beta} - ik^* C_{\alpha\beta}| = 0 \tag{69}$$

where

$$H_{\alpha\beta} = -\int_\Omega \left(\Phi_\alpha \epsilon_{mn} \bar{u}_{n,mj} \epsilon_{jk} \Phi_{\beta,k} + \bar{u}_j \Phi_{\alpha,j} \Phi_{\beta,ii} + \frac{1}{Re} \Phi_{\alpha,ij} \Phi_{\beta,ij} \right) d\Omega \tag{70}$$

where, Φ_α is chosen as the Hermite polynomial bicubic rectangular elements. As a result of this step, we then compute $\hat{u}_i^*$ from

$$\hat{u}_i^* = \epsilon_{ij} \phi_{,j} \tag{71}$$

In addition to these data, we require the eigenvalue analysis of the entire domain to determine natural frequencies k_N and corresponding pressure amplitudes $\hat{P}_N$ from Eqs. (24) and (25). This leads to the finite element analog,

$$|C_{\alpha\beta} - k_N A_{\alpha\beta}| = 0 \tag{72}$$

where the complex dimensionless frequency given by Eq. (18) and $A_{\alpha\beta}$ and $C_{\alpha\beta}$ are shown in Eq. (68a) and Eq. (68c), respectively.

With these data, $\bar{u}_i$, $\hat{u}_i^*$, k_N, and $\hat{P}_N$ are now available, we compute from Eqs. (34) and (35) the acoustic instability growth constants α_A and the acoustically coupled vortical instability growth constants α_H, respectively.

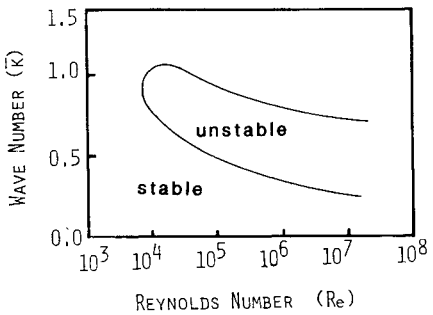

a) Stability boundary in simple model: solutions of Orr-Sommerfeld equation with parabolic mean velocity profile, 24 Hermite polynomial finite elements.

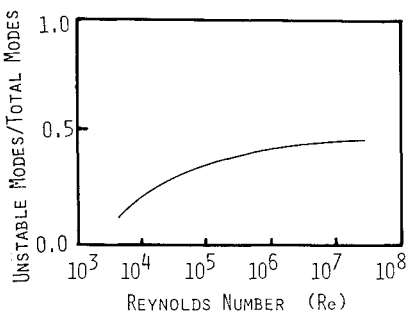

b) Ratio of the number of unstable vortical modes to the total number of vortical modes in simple model: solutions of general vortical disturbance equation with parabolic mean velocity profile, 16 Hermite polynomial bicubic rectangular finite elements.

Fig. 5 Comparisons of the solutions of Orr-Sommerfeld equation and general vortical disturbance equation. The qualitative trends of instability with respect to the Reynolds number are the same in both cases, as seen by the variation of Fig. 5b coinciding with the wavenumber gap of unstable region in Fig. 5a.

IV. Discussion

Simple Model

As described in Sec. III, our objective here is to calculate in a two-dimensional geometry the disturbed vortical component of the stream function amplitudes and, subsequently, the acoustically coupled vortical growth constants. The disturbed stream functions prevail in either stable or unstable vortical modes as shown, respectively, in Figs. 2 and 3. Notice that the disturbed streamlines in stable vortical modes ($\alpha<0$) indicate large vortices formed near the wall that gradually diminish as time elapses. However, in the case of unstable vortical modes ($\alpha>0$), the vortices near the wall spread over the entire domain, moving toward turbulence. Figure 4 shows the growth constants vs Strouhal numbers, with the pronounced amplification of growth constants when vortical disturbances as coupled with acoustic disturbances.

It follows from these observations that the presence of acoustic oscillations in the vortically unstable field give rise to either damping or amplification for the vortical oscillations as a function of Strouhal and Reynolds numbers. It is further seen that it is inconsistent to merely compute the acoustic energy converted from vortical oscillations and attempt to determine acoustic instability independently. Rather, various vortical and acoustic frequencies coexist and they are coupled into either damping or amplification processes as an integrated system from which the combined stability or instability emerges. Thus, we ask: at what combinations of acoustic and vortical frequencies, which are excited, will this coupling action tend to amplification? The answer to this question in the real geometry and practical applications is our ultimate goal.

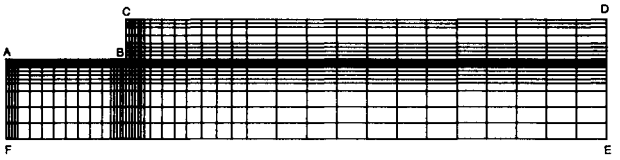

Fig. 6 Finite element meshes in complex model, 832 nodes, 762 bilinear finite elements. Boundary conditions for mean velocity are along AB, $u=-0.01$ (side burning), $u=0.0$ (end burning), $v=0.0$; along BC, $u=0.0$, $v=0.0$; along CD, $u=0.0$, $v=0.0$; along DE, $\partial u/\partial x=0.0$, $v=0.0$; along EF, $\partial u/\partial y=0.0$, $v=0.0$; along FA, $u=0.0$ (side burning), $u=1-\gamma^2$ (end burning), $v=0.0$.

In Fig. 5a, the results of the Orr-Sommerfeld equation are used to construct the classical stability boundaries. It is interesting to note that solution of the general vortical disturbance equation (48), plotted for the ratio of the unstable modes to the total number of modes vs Reynolds numbers (Fig. 5b), shows a qualitative resemblence to the Orr-Sommerfeld stability boundaries. This is seen by the fact that the ordinate of the curve in Fig. 5b corresponds to the ordinate of the unstable region of Fig. 5a.

Complex Model

The finite element calculation of Eqs. (34) and (35) is the highlight of this model. However, we must first determine the mean flow and acoustic and vortical modes as described in Sec. III. Figure 6 shows the finite element meshes and boundary conditions for the mean velocity computation. Figures 7–10 show the vector representation of the mean velocity field and streamlines for $Re=10^3$, 10^4, and 10^5, with the end and side burning propellants in the stepped cylindrical combustion chamber. Note that, for the side burning motor, a secondary flow occurs in the case of a high Reynolds number ($Re=10^5$), as one would expect. See Fig. 10. The results indicate formation of vortex fields due to separation of flow at the corner of the step.

The natural acoustic modes, as a result of finite element solutions of Eqs. (24) and (25), are shown in Fig. 11 for selected acoustic frequencies. Notice that irregular geometries (step cylinder) give rise to irregular low-frequency longitudinal modes. Furthermore, it is seen that radial modes begin to emerge with an increase of frequency.

Figure 12 shows the temporal growth streamline distributions in unstable vortical modes as identified by the positive imaginary part of eigenvalue solutions using the Orr-Sommerfeld equation and the stream function equation (59), with $Re=10^4$ and $\bar{k}=1$. It is seen that unstable vortices spread along entire free shear layers as time elapses. In contrast, the spatial growth streamline distributions are shown in Fig. 13, indicating that the streamlines tend to be unstable toward downstream, being critical in the Strouhal number range of 0.2–0.25, as verified by Michalke.[14] These calculations have been carried out to gain insight into the free shear layer behavior as hypothesized in Refs. 12–15. Obvious limitations, however, are: 1) actual geometries in practice cannot be represented; 2) the hyperbolic tangent velocity profile may not be valid in practical geometries; 3) the vortical mode in the longitudinal direction should not be constant, as assumed in the temporal growth theory; and 4) the vortical disturbances should not grow indefinitely toward downstream. Furthermore, the so-called broadband amplification effect of inviscid vortex shedding[12-15,20] over the Strouhal number range $S=0$–0.5, with $S\simeq 0.2$ being the peak, will be severely distorted when the vortical field interacts with an established acoustic field. It would be quite logical to assert that, in the presence of complicated mean flows and wall effects as well as the acoustic field, stability is governed by many variables. For example, let us examine the calculations by means of finite element Navier-Stokes solu-

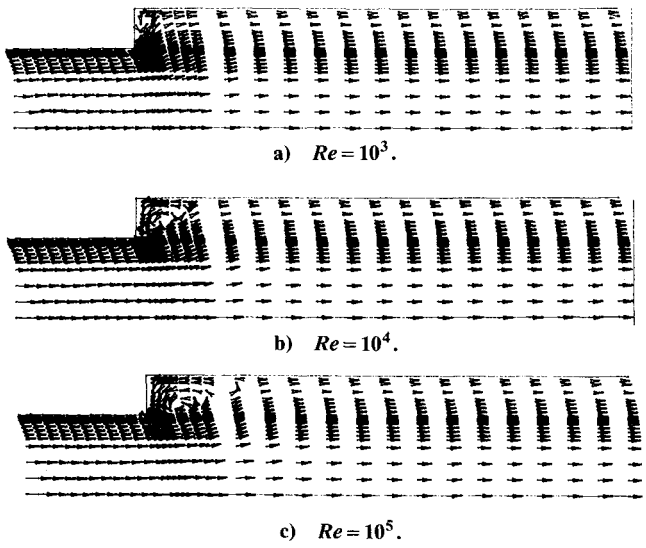

a) $Re = 10^3$.

b) $Re = 10^4$.

c) $Re = 10^5$.

Fig. 7 Mean velocity distribution in end burning motor: solutions of Navier-Stokes equations using 767 bilinear finite elements.

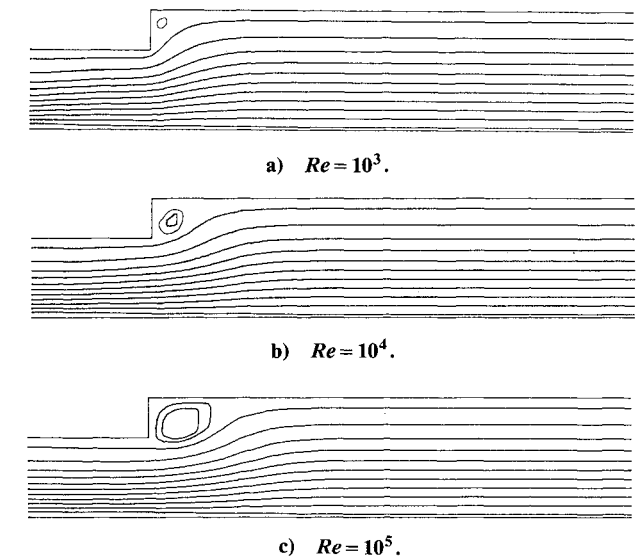

a) $Re = 10^3$.

b) $Re = 10^4$.

c) $Re = 10^5$.

Fig. 8 Streamlines of mean velocity field in end burning motor corresponding to Fig. 7: solutions of Navier-Stokes equations using 767 bilinear finite elements (recirculating region grows with an increase in Reynolds number).

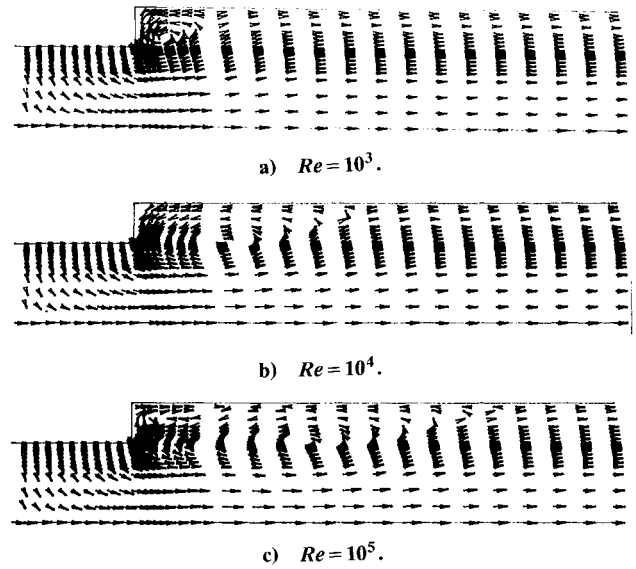

a) $Re = 10^3$.

b) $Re = 10^4$.

c) $Re = 10^5$.

Fig. 9 Mean velocity distribution in side burning motor: solutions of Navier-Stokes equations using 767 bilinear finite elements.

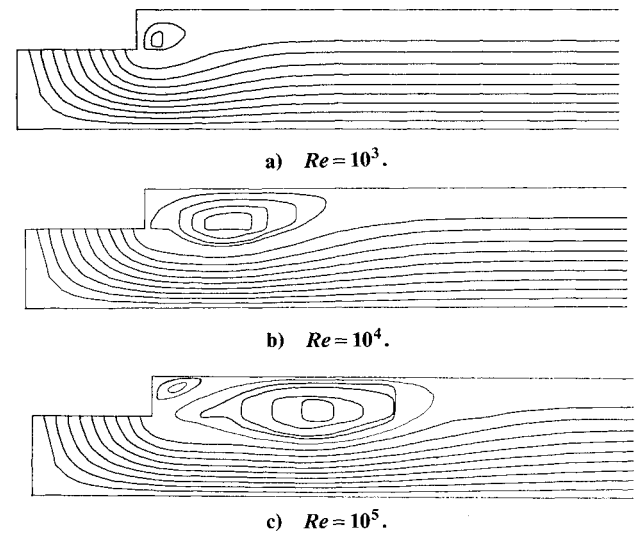

a) $Re = 10^3$.

b) $Re = 10^4$.

c) $Re = 10^5$.

Fig. 10 Streamlines of mean velocity field in side burning motor corresponding to Fig. 9: solutions of Navier-Stokes equations using 767 bilinear finite elements (recirculating region grows with an increase in Reynolds number; recirculating regions are larger than the end burning motor at same Reynolds numbers; secondary recirculating region is found at $Re = 10^5$, expected to affect instability).

tions with the vortical component of velocity from the Orr-Sommerfeld equation leading to the growth constants vs Strouhal numbers, as plotted in Figs. 14 and 15. Here, we note that there is a strong dependency of the growth constants upon the Reynolds numbers and the acoustic frequencies. Thus, the classical broadband amplification effect does not govern the acoustically coupled vortical stability. From Fig. 14 ($\omega_N = 38$ Hz, first acoustic mode, $\bar{k} = 1$), it follows that there are pronounced acoustic-vortical coupling effects in the region of $0.4 < S < 0.6$, being more unstable at higher Reynolds numbers. For $\omega_N = 256$ Hz (fourth acoustic mode), $\bar{k} = 1$, as shown in Fig. 15; such a trend, however, is less evident at high Reynolds numbers as compared with the case of the lower acoustic frequency shown in Fig. 14.

We are now prepared to discuss the main topic of this paper—calculation of growth constants by means of the general vortical disturbance equation (49) as well as the mean flow calculation with Navier-Stokes equations. The growth constants, as calculated from Eqs. (34) and (35), are displayed in Table 1 for $Re = 10^4$ and for selected acoustic frequencies and Strouhal numbers, with individual terms A–G as identified in Eqs. (34) and (35). As expected, the surface combustion term A contributes to the gain of acoustic energy. For $Re = 10^4$, the effect of surface viscous damping C, momentum viscous damping F, and dissipative energy G is negligible, although it tends to play significant roles for low Reynolds number flows. The surface convection term B, often known as "flow turning,"[6] results in amplification of acoustic energy. The flow turning effects are also evident in the energy D and momentum E convection in the domain terms that are not considered in the existing combustion stability code.[21] These terms contribute to not only the loss, but also the gain of acoustic energy, that depend upon the mean velocity (or mean vorticity) distributions and acoustic

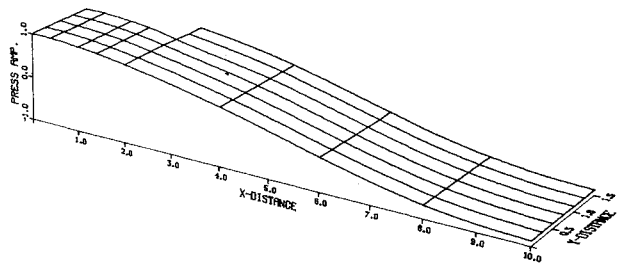

a) First acoustic mode ($\omega_N = 38$ Hz).

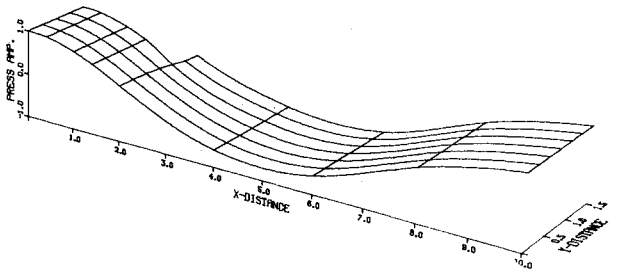

b) Second acoutic mode ($\omega_N = 92$ Hz).

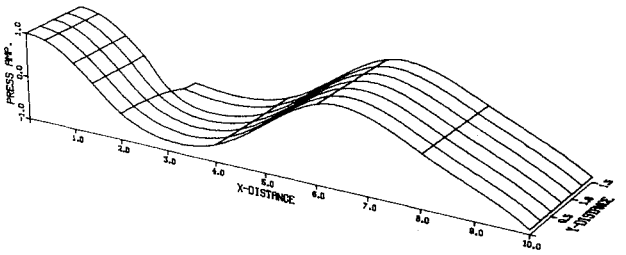

c) Third acoustic mode ($\omega_N = 187$ Hz).

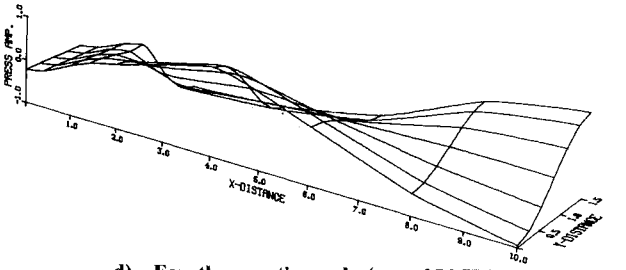

d) Fourth acoustic mode ($\omega_N = 256$ Hz).

Fig. 11 Natural acoustic modes in complex model: solutions of homogeneous Helmholtz equation (24) using 40 bilinear finite elements. Longitudinal modes are pronounced at low natural acoustic frequencies with radial modes activated at high natural acoustic frequency and mode shapes tend to be unsymmetric due to irregular geometry.

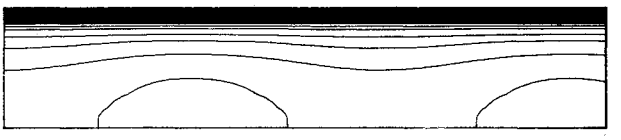

a) $t = 0.0$.

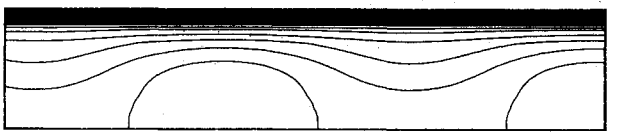

b) $t = 50.0$.

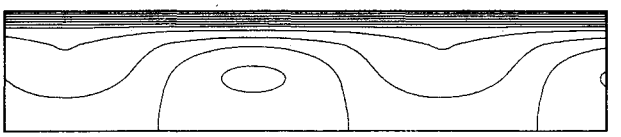

c) $t = 100.0$.

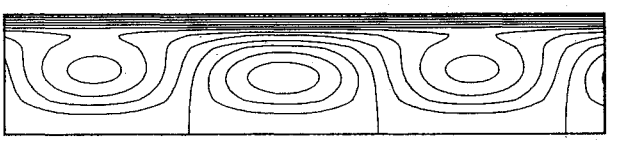

d) $t = 150.0$.

Fig. 12 Complex model temporal growth streamline distributions in unstable vortical modes [the positive imaginary part of eigenvalue solutions in Orr-Sommerfeld equation defines unstable motions, streamlines calculated from Eq. (59) with hyperbolic tangent velocity profile], $Re = 10^4$, $\bar{k} = 1.0$, 48 Hermite polynomial linear finite elements.

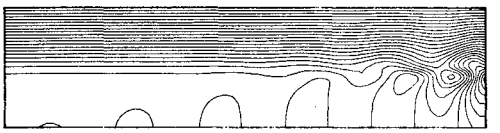

a) $S = 0.15$.

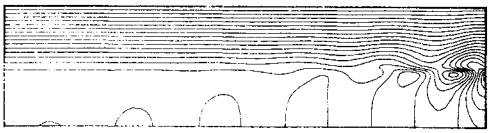

b) $S = 0.25$.

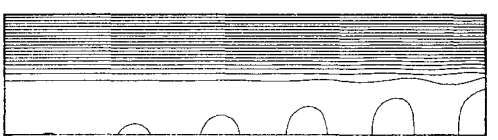

c) $S = 0.35$.

Fig. 13 Complex model spatial growth streamline distributions in unstable vortical modes [the negative imaginary part of eigenvalue solutions in Orr-Sommerfeld equation defines unstable motions, streamlines calculated from Eq. (59) with spatial growth and hyperbolic tangent velocity profile], inviscid case, fourth-order Runge-Kutta method after Michalke.[22]

mode shapes. Therefore, the mean flow/acoustic interaction can be considered by the sum of surface convection term B, energy convection in domain term D, and momentum convection in domain term E.

To evaluate the trends of coupled acoustic and vortical instability phenomena in comparison with semianalytical or simplified processes displayed in Figs. 2-4, 12, and 13, we present the plots of growth constants vs Strouhal numbers and the corresponding stability boundaries in Figs. 16-19. Once again, the first ($\omega_N = 38$ Hz) and fourth ($\omega_N = 256$ Hz) acoustic modes will be considered. A glance at Fig. 16 indicates that the vortical growth constants remain close to zero for the first acoustic mode, whereas more irregular variations are evident for the fourth mode (Fig. 17) in comparison to the case of the temporal growth theory. This trend is a clear indication of the vortical disturbance contribution as determined from the general vortical disturbance equation (48) rather than from either the simplified Orr-Sommerfeld or the inviscid Rayleigh equation. The corresponding stability boundaries, as presented in Figs. 18 and 19, demonstrate the most interesting aspect of the coupling mechanism of acoustic and vortical wave oscillations, in contrast to the classical vortical stability boundary of the Orr-Sommerfeld equation (Fig. 5a). It is seen that, for a given acoustic frequency, there exist multiple islands of stability

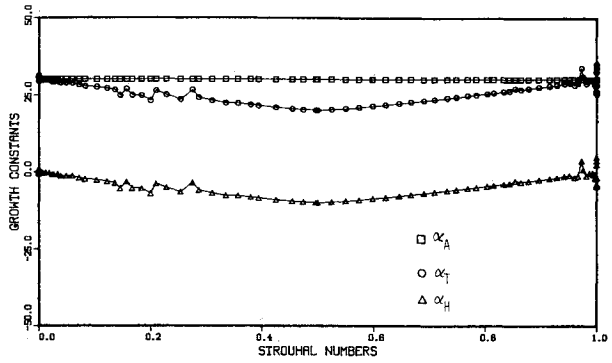

a) $Re = 10^3$.

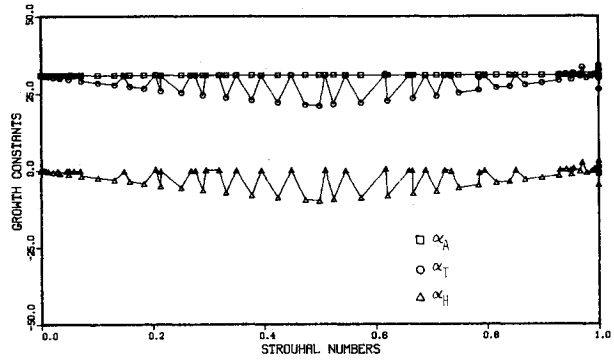

b) $Re = 10^4$.

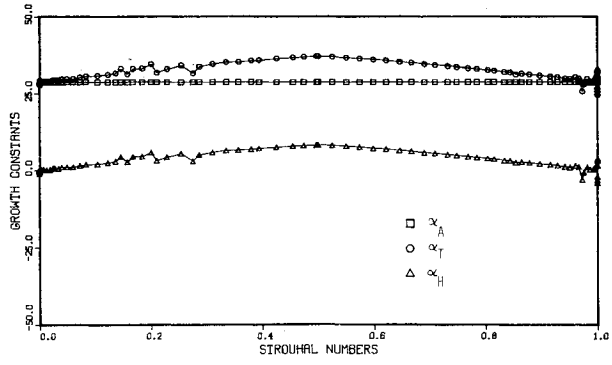

c) $Re = 10^5$.

Fig. 14 Growth constants vs Strouhal numbers in the complex model: temporal growth in Orr-Sommerfeld equation, $\bar{k} = 1.0$, first acoustic mode ($\omega_N = 38$ Hz), pronounced acoustic-vortical coupling effects in the region of $S = 0.4 \sim 0.6$, more unstable at high Reynolds number than at low Reynolds number.

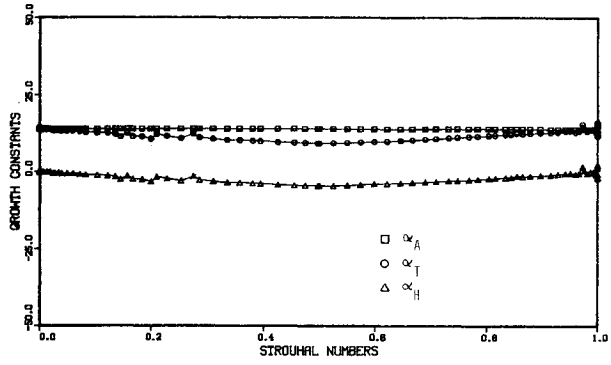

a) $Re = 10^3$.

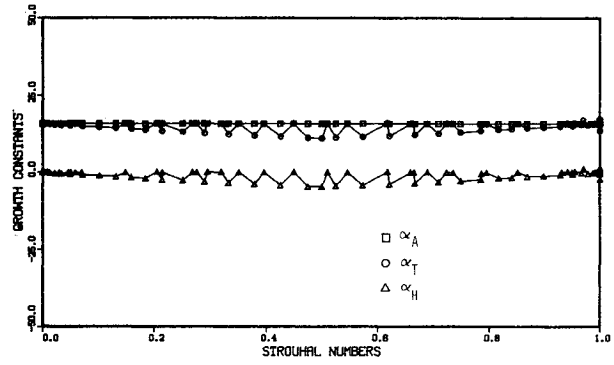

b) $Re = 10^4$.

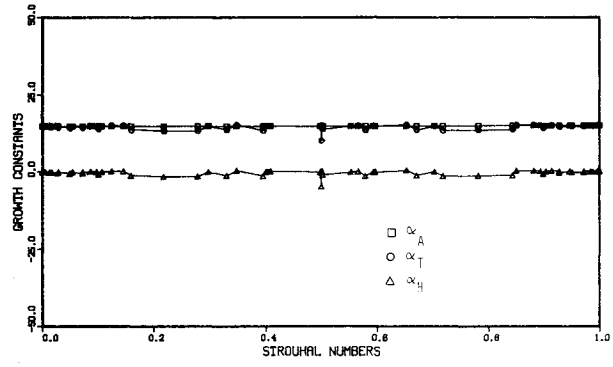

c) $Re = 10^5$.

Fig. 15 Growth constants vs Strouhal numbers in the complex model: temporal growth in Orr-Sommerfeld equation, $\bar{k} = 1.0$, fourth acoustic mode ($\omega_N = 256$ Hz), pronounced acoustic-vortical coupling effects in the region of $S = 0.4$-0.6, more unstable at high Reynolds number than at low Reynolds number. This trend is less pronounced at high Reynolds number compared with the case of first acoustic mode.

Table 1 Growth constants for complex model, $Re = 10^4$, with general vortical disturbance equation

Acoustic frequency, Hz	Strouhal no.	α, s^{-1}	Surface combustion, A	Surface convection, B	Surface viscous damping, C	Energy convection in domain, D	Momentum convection in domain, E	Momentum viscous damping, F	Dissipative energy, G	Sum	α_T
38	0.45	α_A	26.306	10.141	0.0	−1.589	−3.961	0.0	—	30.897	30.448
		α_H	—	0.0	0.0	—	−0.815	0.0	0.0	0.366	
	1.22	α_A	26.306	10.141	0.0	−1.589	−3.961	0.0	—	30.897	30.308
		α_H	—	0.0	0.0	—	0.589	0.0	0.0	0.589	
256	0.45	α_A	0.156	0.002	0.0	18.460	−2.859	0.0	—	15.759	5.117
		α_H	—	0.0	0.0	—	−10.642	0.0	0.0	−10.642	
	1.22	α_A	0.156	0.002	0.0	18.460	−2.859	0.0	—	15.759	23.189
		α_H	—	0.0	0.0	—	7.430	0.0	0.0	7.430	

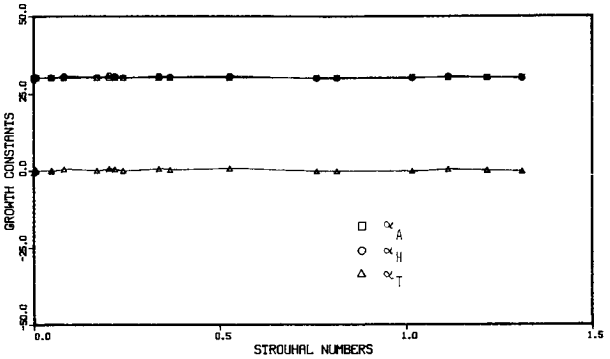

a) $Re = 10^3$.

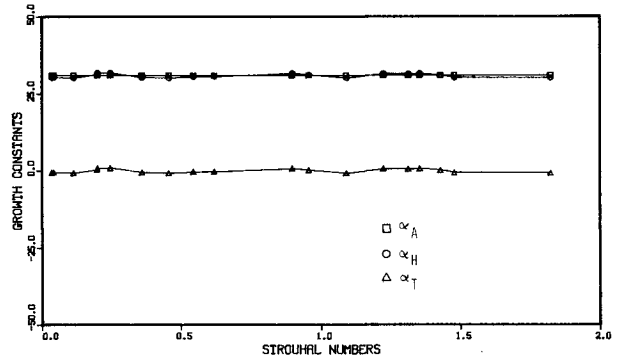

b) $Re = 10^4$.

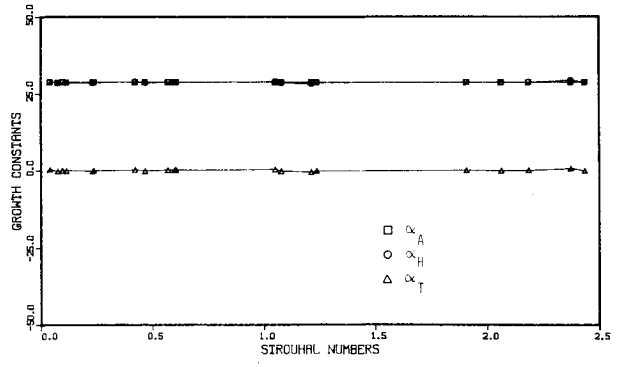

c) $Re = 10^5$.

Fig. 16 Growth constants vs Strouhal numbers in the complex model: vortical modes calculated from general vortical disturbance equation with mean velocity analyzed using finite elements, first acoustic mode ($\omega_N = 38$ Hz), vortical growth constants remain close to zero for the first acoustic mode; no simplifying assumptions imposed in this analysis.

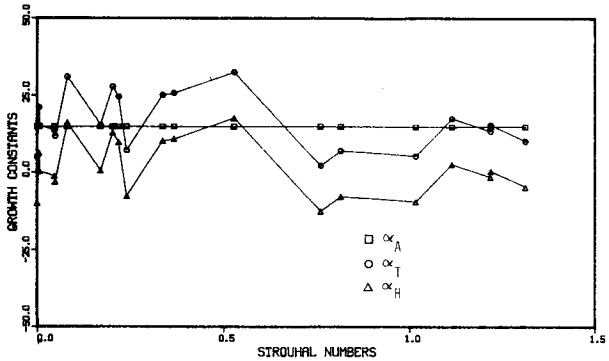

a) $Re = 10^3$.

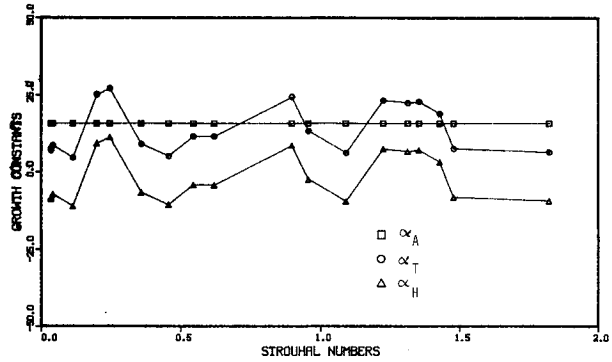

b) $Re = 10^4$.

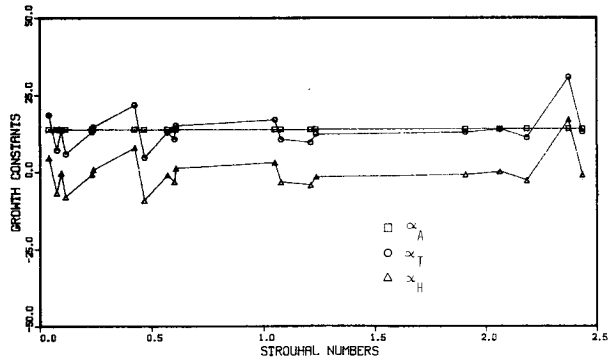

c) $Re = 10^5$.

Fig. 17 Growth constants vs Strouhal numbers in complex model: vortical modes calculated from general vortical disturbance equation with mean velocity analyzed using finite elements, fourth acoustic mode ($\omega_N = 256$ Hz). More irregular variations are evident in comparison with the case of temporal growth approximations (Fig. 15).

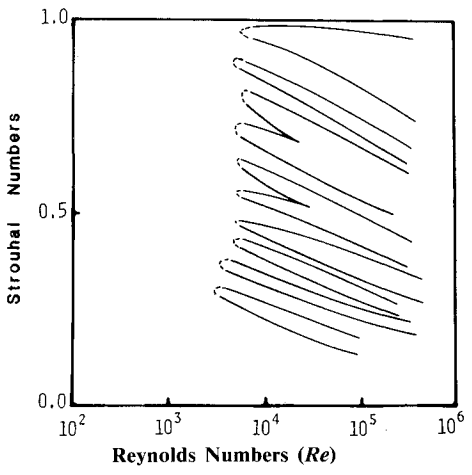

Fig. 18 Stability boundary curves for vortically coupled acoustic growth constants (α_H) in complex model, inside multiple islands unstable, vortical modes calculated from the temporal growth theory of Orr-Sommerfeld equation, $\bar{k} = 1.0$, fourth acoustic mode ($\omega_N = 256$ Hz), corresponding to Fig. 15, multiple islands of stability boundaries with numerous bay areas, unstable areas with Reynolds number larger than approximately 10^3; dotted areas indicate unstable regions.

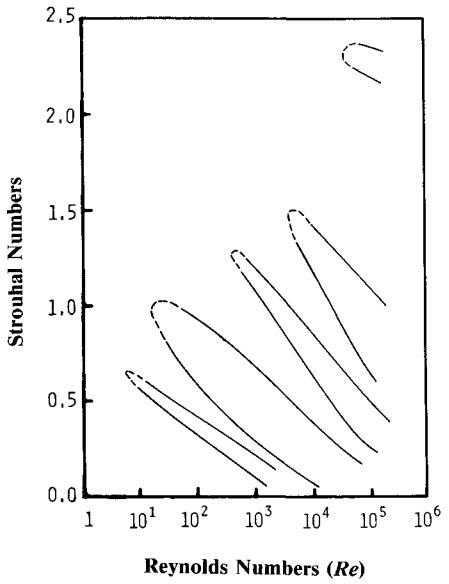

Fig. 19 Stability boundary curves for vorticity coupled acoustic growth constants (α_H) in complex model, inside multiple islands unstable, vortical modes calculated from general vortical disturbance equation with mean velocity analyzed using finite elements, fourth acoustic mode ($\omega_N = 256$ Hz) corresponding to Fig. 17, multiple islands of stability boundaries with numerous bay areas, critical Reynolds number appears to be approximately 10, unstable regions occurring at low Strouhal number are associated with low Reynolds number, this trend continues toward larger Strouhal and Reynolds numbers; dotted areas indicate unstable regions.

boundaries. As a consequence of the interaction of two distinctly different frequencies, acoustic and vortical, the by-product suggests either damping or amplification. They may cancel each other (damping in this case) or help each other to move toward a more unstable position (amplification). The possiblity of damping is indicated by the presence of numerous bay areas. The inapplicability of the broadband amplification effect of free shear layers is demonstrated again in this process of interaction between the acoustic and vortical oscillations. Instability spreads over large ranges of Strouhal and Reynolds numbers. The critical Reynolds numbers for the first and fourth acoustic modes appear to be 5000 and 10, respectively.

Discussions carried out so far are limited to a linear stability. For nonlinear waves such as steep-fronted waves,[19] higher-order perturbation analyses are required. This is a subject for future research.

V. Conclusions

In the course of examining the coupling mechanism of acoustic and vortical wave oscillations, a number of interesting features involved in the analysis of unstable motions of a rocket motor combustion chamber have been brought to light, as follows:

1) The direct superposition of acoustic and vortical components of velocity leads to a physical coupling of two distinctly different wave oscillations in the manner of three-dimensional linear stability.

2) The coupling of both acoustic and hydrodynamic (vortical) components results in an infinite number of combinations of acoustic and vortical frequencies with which various acoustic and hydrodynamic modes are activated. It is shown that the dominance of each contribution or the influence of one upon the other depends on geometries and boundary conditions of the domain of study.

3) The mathematical formulation permits the calculation of growth constants as a sum of acoustic and hydrodynamic contributions. Acoustic frequencies and the mean flow affect both acoustic and hydrodynamic growth constants.

4) Convection terms in the Navier-Stokes equation lead to the most dominant contributions for instability in both the surface and domain integrals, which are absent in the existing stability codes. These terms are found to be critical when rigorous mean flow calculations using finite elements are implemented.

5) For a given acoustic frequency, plots of hydrodynamic growth constants vs vortical frequencies for various Reynolds numbers make it possible to construct stability boundaries. Unlike the stability boundaries of the Orr-Sommerfeld type, which are restricted to parallel flow for transition to turbulence, there exist multiple boundary islands with stable regions in between or interior to the unstable islands, indicating that the coupling mechanism of acoustic and hydrodynamic wave oscillations leads to both amplification and damping throughout all combinations of acoustic and hydrodynamic frequencies.

6) Various semianalytical approaches, such as spatial and temporal growth theories for free shear layers, have been investigated in comparison with the present theory. The inadequacy of these simplified theories for use in coupled acoustic and vortical oscillations has been proved.

7) For finite amplitude oscillations with steep-fronted waves, higher-order perturbations would be required to handle the nonlinearity, the subject of future study.

Acknowledgments

This research was supported partially by the U. S. Army MICOM and NASA/MSFC under DAA H01-85-P-4931 and NAS8-35052, respectively.

References

[1]Schlichting, H., *Boundary Layer Theory*, McGraw-Hill Book Co., New York, 1979.

[2]Crocco, L. and Chen, S. I., "Theory of Combustion Instability in Liquid Propellant Rocket Motors," AGARDograph, No. 8, Butterworth Scientific Publication, London, 1956.

[3]Cantrell, R. H. and Hart, R., "Interaction Between Sound and Flow in Acoustic Cavities: Mass, Momentum, and Energy Considerations," *Journal of the Acoustical Society of America*, Vol. 36, April 1964, pp. 697-706.

[4]Price, E. W., "Review of the Combustion Instability Characteristics of Solid Propellants," *Advances in Tactical Rocket Propulsion*, AGARD, 1965, pp. 143-194.

[5]Culick, F. E. C., "The Stability of One-Dimensional Motions in a Rocket Motor," *Combustion Science and Technology*, Vol. 7, 1973, pp. 165-175.

[6]Culick, F. E. C., "Stability of Three-Dimensional Motions in a Combustion Chamber," *Combustion Science and Technology*, Vol. 10, 1975, pp. 109-124.

[7]Flandro, G. A. and Jacobs, H. R., "Vortex Generated Sound in Cavities," AIAA Paper 74-1014, 1973.

[8]Culick, F. E. C. and Magiawala, K., "Excitation of Acoustic Modes in a Chamber by Vortex Shedding," *Journal of Sound and Vibration*, Vol. 64, No. 3, 1979, pp. 455-457.

[9]Mason, D. R., Folkman, S. L., and Behring, M. A., "Thrust Oscillations of the Space Shuttle Solid Rocket Booster Motor During Static Tests," AIAA Paper 79-1138, 1979.

[10]Brown, R. S. et al., "Vortex Shedding Studies," AFRPL TR-79-244; also AIAA Paper 80-1092, 1980.

[11]Yates, J. E., "Interaction with/and Production of Sound by Vortex Flows," AIAA Paper 77-1352, 1977.

[12]Michalke, A., "On the Inviscid Instability of the Hyperbolic Tangent Velocity Profiles," *Journal of Fluid Mechanics*, Vol. 9, 1964, pp. 543-556.

[13]Michalke, A., "Vortex Formation in a Free Boundary Layer According to Stability Theory," *Journal of Fluid Mechanics*, Vol. 22, Pt. 2, 1965.

[14]Michalke, A., "On Spatially Growing Disturbances in an Inviscid Shear Layer," *Journal of Fluid Mechanics*, Vol. 25, Pt. 4, 1966, pp. 521-554.

[15]Freymuth, P., "On Transition in a Separated Laminar Boundary Layer," *Journal of Fluid Mechanics*, Vol. 25, Pt. 4, 1966, pp. 683-704.

[16]Chung, T. J. and Sohn, J. L., "Coupled Acoustic and Hydrodynamic Wave Instabilities," *21st JANNAF Combustion Meeting*, Vol. 1, Oct. 1984, pp. 129-137.

[17]Chung, T. J., *Finite Element Analysis in Fluid Dynamics*, McGraw-Hill Book Co., New York, 1978.

[18]Morse, P. M. and Feshback, H., *Methods of Theoretical Physics*, Pts. I and II, McGraw-Hill Book Co., New York, 1953.

[19]Baum, J. D., Lovine, R. L., and Levine, J. N., "Pulsing of Solid Propellant Rocket Motors: Modeling and Cold Flow Testing," AIAA Paper 82-0359, 1982.

[20]Flandro, G. A. et al., "Internal Flow Field Investigation," AFRPL-TR-85-079, Oct. 1985.

[21]Lovine, R. L., "Standard Stability Prediction Method for Solid Rocket Motors," Vol. 1, Final Report, AFRPL-TR-76-32, May 1976.